



# Analysis and optimization for energy, cost and carbon emission of a solar driven steam-autothermal hybrid methane reforming for hydrogen, ammonia and power production

H. Ishaq<sup>\*</sup>, I. Dincer

Clean Energy Research Laboratory, Faculty of Engineering and Applied Science, University of Ontario Institute of Technology, 2000 Simcoe Street North, Oshawa, Ontario, L1H 7K4, Canada

## ARTICLE INFO

### Article history:

Received 22 April 2019

Received in revised form

30 May 2019

Accepted 3 June 2019

Available online 8 June 2019

### Keywords:

Efficiency

Hydrogen production

Solar energy

Ammonia synthesis

Cost analysis

CO<sub>2</sub> capturing

## ABSTRACT

A novel idea of solar driven steam-autothermal hybrid reforming system (SAHRS) is proposed with onboard carbon capturing system in the existence of carbon emissions taxes. The CO<sub>2</sub> produced by the steam methane reforming is employed to the autothermal reforming as input and cryogenic air separation unit is integrated to provide autothermal reforming with oxygen and ammonia synthesis with nitrogen. The autothermal reforming is modified with further integration of water gas shift reactor (WGSR) which converts carbon mono-oxide into carbon dioxide by reacting with steam and this CO<sub>2</sub> is captured in the carbon capturing system using aqueous ammonia. Some amount of hydrogen produced by the autothermal reforming is employed to the ammonia synthesis reactor to achieve onboard ammonia for CO<sub>2</sub> capture. The system generates enough power to overcome the required power and supply power as a final commodity as well. The present system is essentially designed for cleaner production and industrial applications. The performance indicator for the designed system is defined in terms of energy and exergy efficiencies which are found to be 53.4% and 45.0% respectively. The carbon emissions produced by the system and tax saving by the aqueous ammonia based CO<sub>2</sub> capturing are also calculated in the proposed study.

© 2019 Elsevier Ltd. All rights reserved.

## 1. Introduction

The gradual depletion of the global fossil fuels reserves has been requiring critical research, innovation, advancement and technology developments on alternative energy sources, systems and applications. As per the forecast report from the Energy Information Administration (EIA, 2019), the world's energy demand seems to upsurge by 50% by 2030. Wide-ranging research is being conducted on the efficient utilization of fossil fuels of the alternative energy sources because of the restricted fossil fuels nature and their effects on the environment (Jegadheesan et al., 2013; Muradov and Veziroğlu, 2008). The renewable and clean nature of solar energy makes it a strong candidate for research, advancement and development (Ishaq et al., 2018). Numerous researchers consider solar energy as a promising replacement of fossil fuels as energy sources in the future.

A number of researchers (Atif and Al-Sulaiman, 2018; Islam and Dincer, 2017) have developed and analyzed different integrations of solar energy with other systems, where they have integrated Brayton cycles recompression with solar tower and an optimized model of the solar heliostat was employed while in the other study, a solar-geothermal based integrated system was developed and analyzed. This developed system was comprised of two storage systems, a heat pump, two organic Rankine cycles (ORC), a drying system and an absorption chiller and system was developed for multigenerational purposes.

Wang and Naterer (2014) proposed a paper on hydrogen production based on fossil fuel and solar energy and also analyzed the CO<sub>2</sub> mitigation. The higher thermal energy requirement for hydrogen production cycles via endothermic reactions supports the fossil fuel consumption and thus, greenhouse gas emissions. Some of the hydrogen production methods by fossil fuels were considered in this study such as coal gasification, steam methane reforming, methane dissociation and off-gas reforming to analyze the CO<sub>2</sub> emissions. It was established that steam methane reforming carries lesser challenges if the enthalpy of the

<sup>\*</sup> Corresponding author.

E-mail address: [haris.ishaq@uoit.net](mailto:haris.ishaq@uoit.net) (H. Ishaq).

endothermic reaction is delivered by solar energy. [Sheu and Mitsos \(2013\)](#) analyzed a fossil fuel and solar based plant employing the steam methane reforming in combined cycle and also optimized the proposed system. A heuristic approach by utilized for the optimization and results revealed that the integration of the solar tower with steam methane reforming is a promising and favorable integration option. The researchers have proposed the integration of solar energy with some other integrated system as well such as ([Xu et al., 2017](#); [Zheng et al., 2015](#)), where one of the studies was based on the integration of solar energy with coal power generation and also analyzed the CO<sub>2</sub> capturing system while the other study analyzed the solar based steam methane reforming systems. The key objective of this project was to develop a system for commercialization of solar energy based reforming system and to provide high efficiency to assist as a conventional system by 2020.

[Hagh \(2004b\)](#) deliberately worked on the different aspects of the autothermal reforming. In this study, the stoichiometric analysis was conducted for autothermal processing while in another study, the comparison and framework assessment of the autothermal reforming based on the hydrocarbon fuels were conducted. The stoichiometric analysis framework analyzed in this study was also employed to govern the space for reforming reaction with methane, methanol, isooctane, ethanol, propane, and hexadecane. Another study conducted the comparison and framework of the autothermal reforming based on the hydrocarbon fuels ([Hagh, 2004a](#)). [Yan et al., \(2018\)](#) studied the properties of hydrogen producing technique of autothermal reforming in a membrane reactor. The membrane reactor has a better tendency and conversion rate to yield hydrogen. The results revealed that the increase in the molar ratio of air and methane results in lower production of hydrogen. It was also concluded that the autothermal methane reforming takes place more effectively at the temperature of 973K and at the air and methane molar ratio of 1 and 2. [Colucci \(2006\)](#) analyzed the autothermal reforming for hydrogen production using biodiesel and some other fuels. This study was majorly focused upon the fuel cell applications. The objective of this study was to investigate the conversion of biodiesel, methanol and glycerin into hydrogen using a new catalyst and to investigate the production potential, suitable operating conditions, water to carbon ratios and the reactor temperature.

[Raibhole and Sapali \(2012\)](#) conducted the modeling and parametric study on the cryogenic air separation unit in order to employ biomass gasification. As oxygen works as a gasification agent in the biomass gasification, this property helps is many other applications like IGCC, Fischer-Tropsch products and chemical production. The present study integrated the cryogenic air separation unit with biomass gasification reactor and Aspen Plus tool was utilized for the simulation of the proposed design. [Ray \(2015\)](#) utilized the Hampson-Linde Approach for cryogenic air separation. This particular research also explained the functionality of the Linde cycle for cryogenic air separation emphasizing on the oxygen, nitrogen and argon production processes.

[Kim et al. \(2011\)](#) conducted a study on the aqueous ammonia driven carbon capturing technique. In this study, the basic and deep understanding of the CO<sub>2</sub> conversion mechanism was developed with the help of stoichiometric calculations and reaction kinetics. The capturing process was investigated thoroughly and ammonia was found performing as reactant, base, catalyst, and product at the same period of time. Another study conducted better utilization of industrial waste heat recovery and employed it to an integrated system for multiple objectives and also considered carbon capturing ([Ishaq and Dincer 2019](#)). [Wu et al. \(2009\)](#) performed an experimental study on the ammonia and soil mixture based carbon capturing technique. It was also proposed that ammonium bicarbonate (NH<sub>4</sub>HCO<sub>3</sub>) as one of the product components can also be

employed for absorbing CO<sub>2</sub>. It was revealed that the capacity of CO<sub>2</sub> capture by employing this methodology was 15% higher as compared to the summation of physical adsorption capacity soil and chemical absorption capacity ammonia. [Al-Bassam et al. \(2018\)](#) presented a renewable (solar) energy based system of natural gas driven steam methane reforming. This study developed a performance enhanced system of solar driven steam methane reforming by incorporating the steam and carbon mono-oxide which change the endothermicity of the steam methane reforming process. The advanced system was found to be preferable for the usage of natural gas hydrogen production in the existence of substantial taxation levels.

The proposed system uses solar heliostat as an energy source and employs natural gas as fuel for steam and autothermal reforming. The proposed integration develops a new approach for the energetically enhanced integrated system for steam-autothermal hybrid reforming system including onboard carbon capturing. Some part of the heat from the molten salt is transferred to the steam which is employed to the steam-autothermal hybrid reforming system (SAHRS) while remaining heat is provided to the reheat Rankine cycle for power production. The explicit objectives of the proposed study are (i) to develop a solar energy driven natural gas reforming system with carbon capturing, (ii) to introduce a steam-autothermal hybrid reforming system (SAHRS) (iii) to model and simulate the proposed system in Aspen Plus software tool, (iv) to calculate the carbon emissions and tax saving by the aqueous ammonia based CO<sub>2</sub> capturing and (v) conducting different parametric studies to investigate the system's enhanced performance.

## 2. System description

The schematic design of the proposed system is shown in [Fig. 1](#) with the specification of each state point accordingly. The Aspen Plus simulation design of the steam-autothermal methane reforming amended with integration of water gas shift reactor, cryogenic air separation unit and ammonia synthesis reactor is shown in [Fig. 2\(a\)](#), the model of the reheat Rankine cycle is presented in [Fig. 2\(b\)](#) and the aqueous ammonia based carbon capturing system is exhibited in [Fig. 2\(c\)](#). All the major operating parameters such as temperatures, pressures, direct normal irradiance, working fluid and conversion rates are arranged in [Table 1](#). The significant properties of each state point such as temperature, pressure, enthalpy, entropy, flow rate and exergy are displayed in [Table 2](#) while [Fig. 3](#) exhibits the equipment and installation costs for key components. The description of each subsystem is described below.

### 2.1. Solar heliostat field

A solar heliostat field with a number of heliostats is employed as a heat source to the proposed system configuration. The lithium chloride salt is used as a working fluid to transmit the heat from solar heat source to the steam-autothermal reforming and reheat Rankine cycle. The direct normal irradiance assumed for the designed solar heliostat is 800 W/m<sup>2</sup> ([Ishaq et al., 2018](#)). The configuration is designed in a manner to provide the steam-autothermal reforming with mandatory heat and additional heat is employed to the reheat Rankine cycle for power generation.

### 2.2. Natural gas reforming

A steam-autothermal hybrid reforming system is driven by solar energy source. The following are the two types of natural gas reforming:

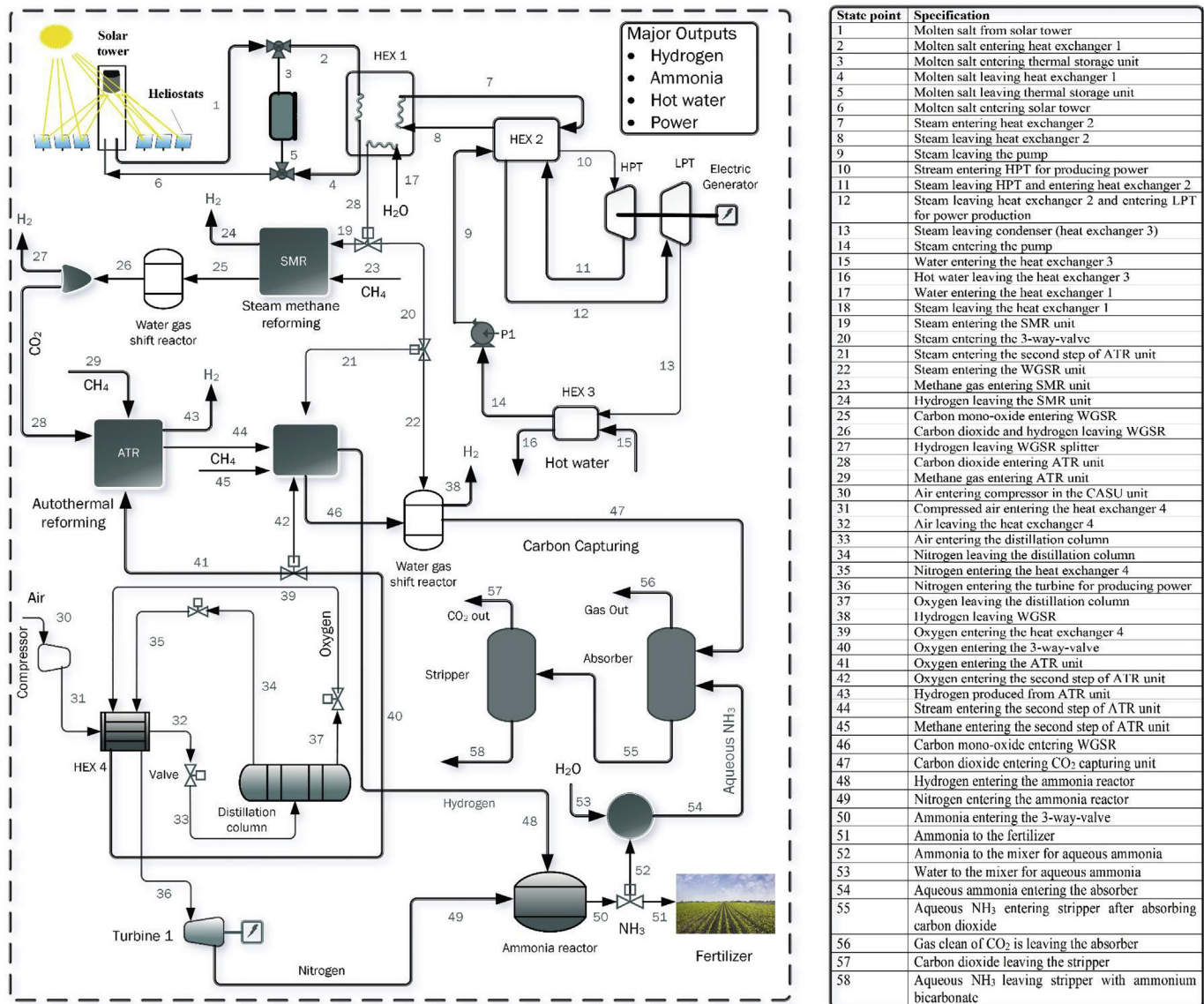


Fig. 1. The solar-methane driven proposed system consisting of steam and autothermal reforming, reheat Rankine cycle, cryogenic air separation unit, ammonia synthesis and carbon capturing.

### 2.2.1. Steam methane reforming (SMR)

Natural gas steam reforming is one of the most communal means of producing hydrogen globally. Hydrogen can be used as an energy carrier, thermal energy, for ammonia synthesis and as electrical energy by fuel cells. Methane reacts with steam at high temperature (B2A) and yields hydrogen and carbon monoxide. In the next step, carbon monoxide reacts with steam in a water gas shift reactor (B2C) to produce hydrogen and carbon dioxide.

### 2.2.2. Autothermal reforming (ATR)

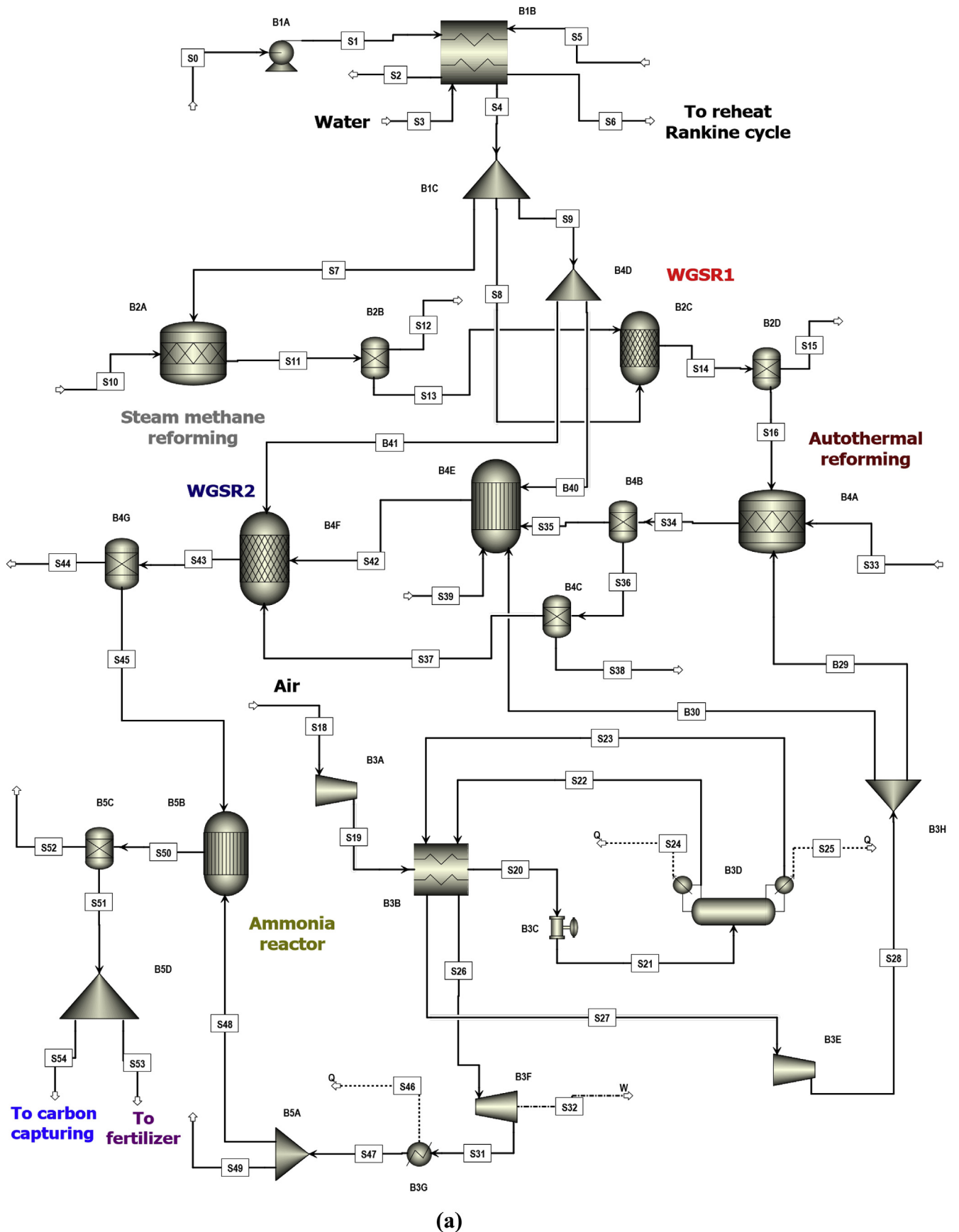
In autothermal reforming, methane reacts with carbon dioxide in the presence of oxygen gas to formulate syngas. In the first step, the autothermal reforming uses carbon dioxide (B4A) and produces hydrogen and carbon monoxide in 1:1 whereas in the second step, the autothermal reforming uses steam (B5E) and produces hydrogen and carbon monoxide in 2.5:1. The performance of autothermal reforming is enhanced by adding a water gas shift reactor (B4F) to convert carbon monoxide into carbon dioxide.

### 2.3. Cryogenic air separation unit (CASU)

The air is compressed via compressor (B3A) before entering the distillation column. Due to the compression, the air temperature rises. The distillation column (B3D) separates oxygen from nitrogen and provides 95% pure oxygen. The produced oxygen compressed towards the autothermal reforming reactors via compressor B3E by transferring the heat to the nitrogen gas and nitrogen gas is supplied to the ammonia reactor (B5B) after been expanded in the turbine (B3F) for synthesizing ammonia.

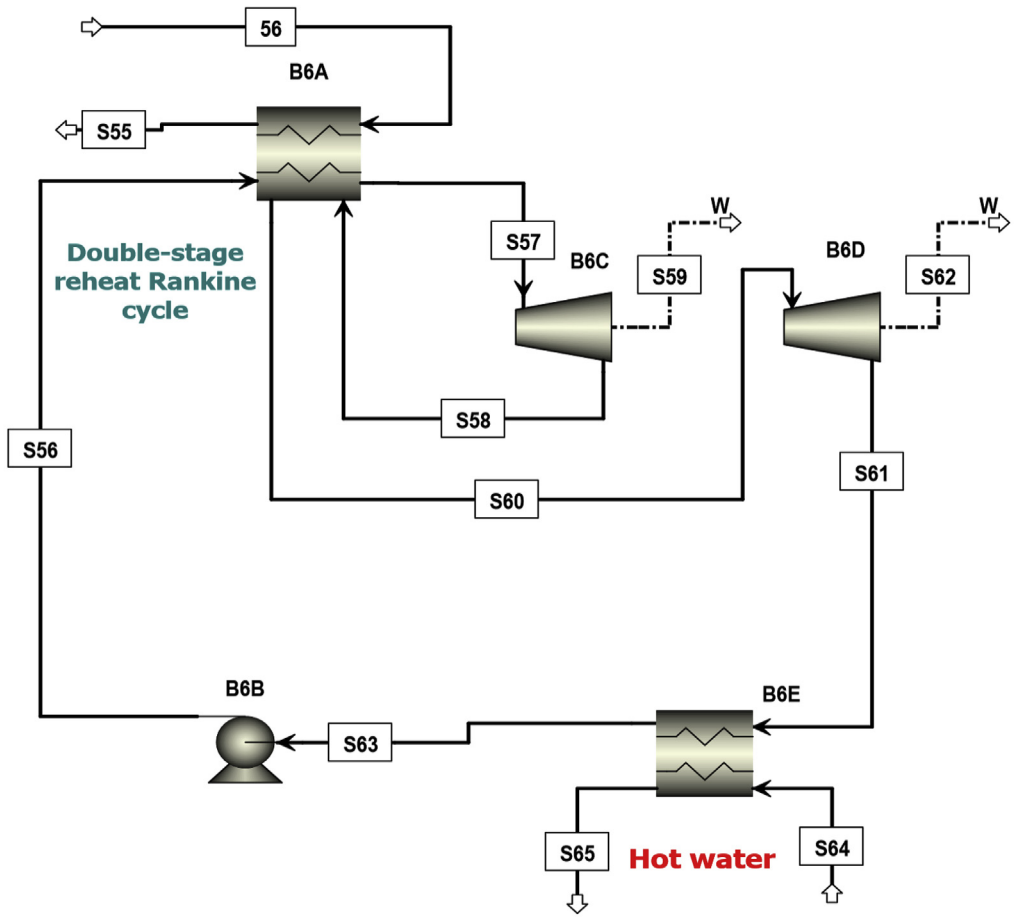
### 2.4. Ammonia synthesis

The hydrogen from the water gas shift reactor (B4F) reaches to the ammonia reactor (B5B) via stream (S45) while nitrogen to the ammonia reactor via stream S48 from the cryogenic air separation unit. The hydrogen reacts with ammonia at high temperature and pressure to synthesize ammonia. The conversion rate of ammonia synthesis reaction is 70%. The unreacted gases are separated

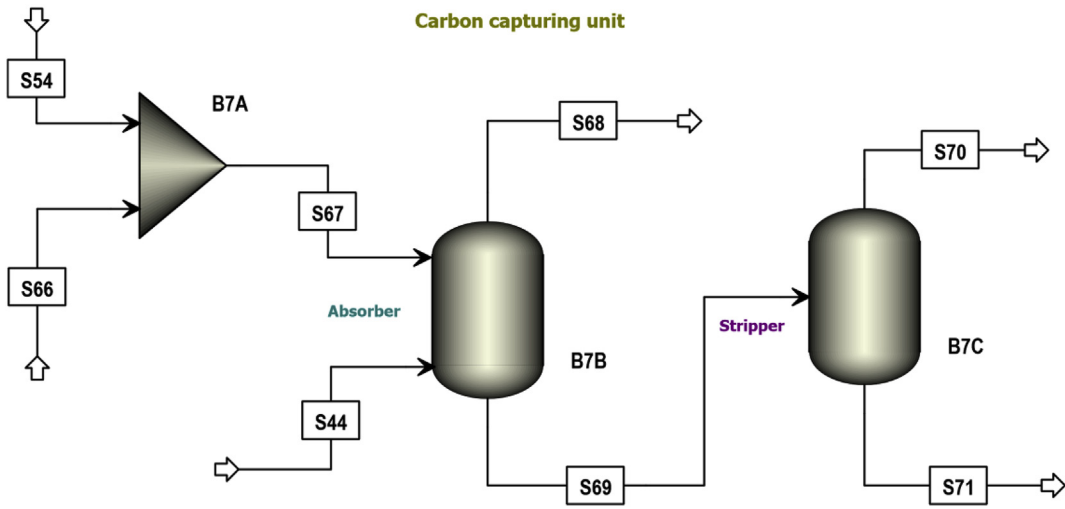


(a)

Fig. 2. (a) Aspen Plus simulation design of the system including steam-autothermal methane reforming, WGSR, ASU and ammonia synthesis reactor, (b) Reheat Rankine cycle coupled with hot water stream and (c) Aqueous ammonia based carbon capturing unit.



(b)



(c)

Fig. 2. (continued).

through a separator (B5C) and a part of synthesized ammonia is sent to the carbon capturing unit while remaining is one of the major commodity of the system.

### 2.5. Reheat Rankine cycle

The additional heat from the molten salt is set to be provided to the reheat Rankine cycle for power generation. The heat exchanger

(B6A) is employed to transfer the heat to the water which is converted into steam and expanded in the turbines (B6C) and (B6D). The working fluid is expanded in two different stages to reduce the temperature difference and thus, exergy destruction. The additional heat from the condenser is used to provide the hot water.

2.6. Carbon capturing unit

The carbon dioxide produced by the autothermal reforming reaches the carbon capturing unit. The ammonia synthesized on board, is converted to the aqueous ammonia and employed for carbon capture. In the first step, the aqueous ammonia absorbs the carbon dioxide in absorber (B7B) by making different by-products like ammonium bicarbonate. The remaining absorbent (aqueous ammonia) and unreacted carbon dioxide are separated in the stripper (B7C).

3. Analysis and assessment

The thermodynamic, cost and carbon emissions analyses are

performed for the solar based integrated system. The thermodynamics analysis performed on the overall system and individual component in presented is this section. The design parameters of each major subsystem such as solar heliostat, steam methane reforming, autothermal reforming and ammonia synthesis are tabulated in Table 1. The design parameters include irradiance, number of heliostats, heliostat mirror area and heliostat efficiency for solar heliostat while the operating conditions of the other subsystems. The following are the general balance equations for energy, entropy and exergy analyses:

$$\dot{Q}_i + \dot{W}_i + \sum_i \dot{m}_i \left( h_i + \frac{V_i^2}{2} + gZ_i \right) = \dot{Q}_e + \dot{W}_e + \sum_e \dot{m}_e \left( h_e + \frac{V_e^2}{2} + gZ_e \right) \tag{1}$$

$$\sum_i \dot{m}_i s_i + \dot{S}_{gen} + \sum_i \left( \frac{\dot{Q}_k}{T_k} \right) = \sum_e \dot{m}_e s_e + \sum_e \left( \frac{\dot{Q}_k}{T_k} \right) \tag{2}$$

$$\sum_i \dot{m}_i ex_i + \dot{E}x^Q + \dot{E}x_w = \sum_e \dot{m}_e ex_e + \dot{E}x_w + \dot{E}x^Q + \dot{E}x_d \tag{3}$$

Here,  $\dot{W}$  denotes work rate,  $\dot{Q}$  signifies heat rate,  $h$  in enthalpy,  $s$  represents entropy,  $ex$  denotes exergy and  $\dot{E}x_d$  shows exergy destruction rates.

Table 1  
Operating parameters of the proposed system.

Design parameters	Value
<b>Solar Heliostat</b>	
Irradiance $\dot{i}_b$	0.8 kW/m <sup>2</sup>
Dimensions of heliostat mirror area	296 m <sup>2</sup>
Number of heliostats $N_{he}$	100
Heliostat efficiency	80%
Working fluid	Molten salt
<b>Steam methane reforming</b>	
SMR reactor temperature	700 °C
SMR reactor pressure	5 bar
<b>Autothermal methane reforming</b>	
ATR reactor temperature	950 °C
ATR reactor pressure	100 bar
<b>Ammonia synthesis</b>	
Ammonia synthesis reactor temperature	350 °C
Ammonia synthesis reactor pressure	50 bar
Ammonia synthesis reactor conversion rate	70%

3.1. Solar heliostat field

The designed system is set to be driven by a solar heliostat field with 100 heliostats. A part of heat is linked with steam-autothermal hybrid reforming system (SAHRS) and additional heat is transferred to the reheat Rankine cycle for power production. The molten salt is used as a working fluid for solar energy input (Siddiqui and Dincer, 2017). The entire system excluding solar heliostat is simulated in Aspen Plus. The operating parameters of the solar heliostat are arranged in Table 1. The correlation used to calculate the solar heat

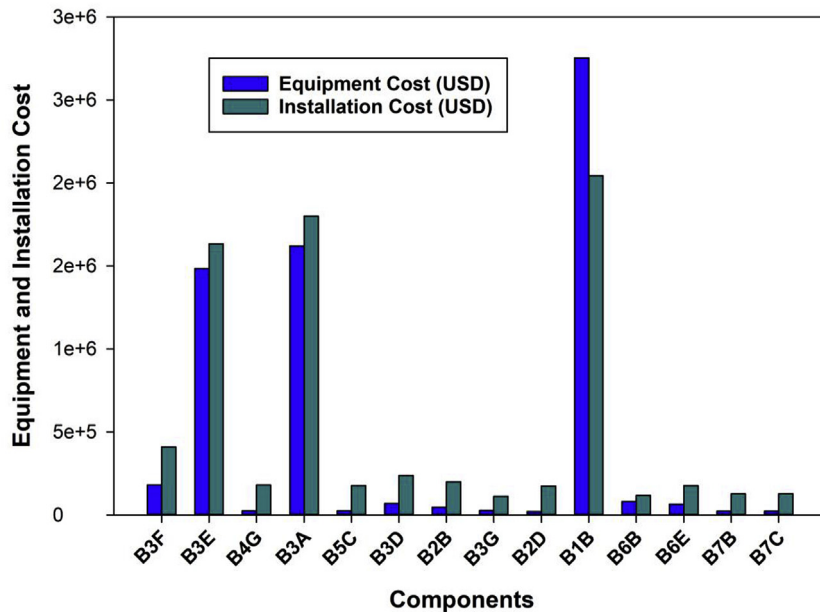


Fig. 3. The costs and weights of the main system components.

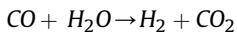
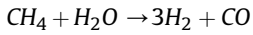
input can be described as follows:

$$\dot{Q}_{solar} = \eta_{he} \dot{I}_b A_{he} N_{he} \quad (4)$$

Here,  $\dot{Q}_{solar}$  is the solar heat,  $A_{he}$  denotes heliostat area,  $\eta_{he}$  is heliostat efficiency,  $N_{he}$  is number of heliostats and  $\dot{I}_b$  is irradiance.

### 3.2. Steam methane reforming

The natural gas steam reforming carried out in this study utilizes the solar heat input for hydrogen production. The chemical reactions included in the steam methane reforming are:



The first step of methane reacting with steam is highly endothermic and carried out at 700 °C and 5 bar. The second step of steam reacting with carbon monoxide in WGSR is carried out at 700 °C and 5 bar and it is slightly exothermic. The reaction kinetics model of [Ding and Alpay \(2000\)](#) is described as follows:

$$R_I = \frac{k_1}{P_{H_2}^{2.5}} (P_{CH_4} P_{H_2O} - P_{H_2}^3 P_{CO}) (DEN)^2 \quad (5)$$

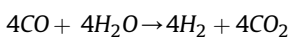
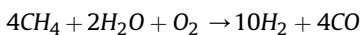
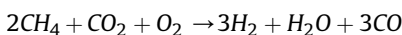
$$R_{II} = \frac{k_2}{P_{H_2}} (P_{CO} P_{H_2O} - P_{H_2} P_{CO_2}) (DEN)^2 \quad (6)$$

$$DEN = 1 + K_{CO} P_{CO} + K_{H_2} P_{H_2} + K_{CH_4} P_{CH_4} + K_{H_2O} P_{H_2O} / P_{H_2} \quad (7)$$

Here,  $R_I$  represents the above mentioned hydrogen production reaction while  $R_{II}$  denotes the water gas shift reaction to convert CO into  $CO_2$ .

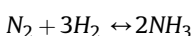
### 3.3. Autothermal reforming

The autothermal methane reforming is carried out using both steam and carbon dioxide in the presence methane and oxygen. The autothermal reforming using carbon dioxide is employed to the reactor (B4A) at 900 °C temperature and 100 bar pressure while autothermal reforming using steam is carried out in the second reactor (B4E). Another step of water gas shift reactor (B4F) is added to the autothermal reforming. The chemical reactions included in the autothermal reforming are written as follows:



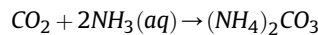
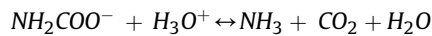
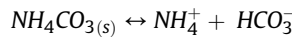
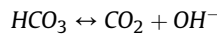
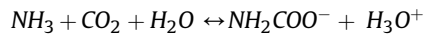
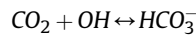
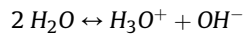
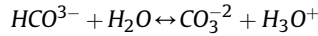
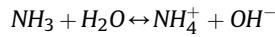
### 3.4. Ammonia synthesis

The partial amount of hydrogen produced by autothermal reforming and WGSR2 is processed through the ammonia reactor (B5B) for ammonia synthesis. The Haber-Bosch method is employed for the ammonia synthesis and conversion rate of 0.7 is considered during the simulation. The chemical reaction for ammonia synthesis can be given as ([Ishaq and Dincer, 2019](#)):



### 3.5. $CO_2$ capturing unit

The ammonia is one of the major commodity of the proposed system and some amount of ammonia is mixed with water, and aqueous ammonia is further utilized for the carbon capturing. The aqueous ammonia is used as absorbent in the absorber (B7B) to capture  $CO_2$ . The by-products like ammonium bicarbonate and unreacted  $NH_3$  are separated from unreacted  $CO_2$ . The chemical reactions accompanying the  $CO_2$  absorption process by an aqueous ammonia specified in Aspen Plus are given as follows:



### 3.6. Overall system assessment

The net heat expression for the proposed system is expressed by the following expression:

$$\begin{aligned} \dot{Q}_{net} = & \dot{Q}_{B1A} + \dot{Q}_{B2A} - \dot{Q}_{B2C} + \dot{Q}_{B4A} + \dot{Q}_{B4E} - \dot{Q}_{B4F} + \dot{Q}_{B3D} \\ & - \dot{Q}_{B3G} - \dot{Q}_{B5B} - \dot{Q}_{B7B} + \dot{Q}_{B7C} \end{aligned} \quad (8)$$

The net amount of work produced by the designed system is as follows:

$$\dot{W}_{net} = \dot{W}_{B6C} + \dot{W}_{B6D} + \dot{W}_{B3F} - \dot{W}_{B1A} - \dot{W}_{B3D} - \dot{W}_{B3A} - \dot{W}_{B3E} \quad (9)$$

The major commodities of the designed system are hydrogen, ammonia, hot water and power. The performance indicator for the proposed system is defined in terms of efficiency and the correlations for energy and exergy efficiencies can be expressed as

$$\eta_{en} = \frac{\dot{m}_{NH_3} LHV_{NH_3} + \dot{m}_{H_2} LHV_{H_2} + \dot{W}_{net} + \dot{m}_{S64} (h_{S65} - h_{S64})}{\dot{Q}_{solar} + \dot{m}_{CH_4} LHV_{CH_4}} \quad (10)$$

$$\eta_{ex} = \frac{\dot{m}_{NH_3} ex_{NH_3} + \dot{m}_{H_2} ex_{H_2} + \dot{W}_{net} + \dot{m}_{S64} (ex_{S65} - ex_{S64})}{\dot{Ex}_{\dot{Q}_{in}} + \dot{m}_{CH_4} ex_{CH_4}} \quad (11)$$

#### 4. CO<sub>2</sub> emissions, carbon fuel taxes and cost analyses

The carbon emissions and cost analyses of the proposed energy system are described in this section.

##### 4.1. Carbon fuel tax saving

As steam and autothermal reforming emit carbon monoxide after combustion which is further converted into carbon dioxide by reacting it with steam, this produced carbon dioxide is captured through aqueous ammonia synthesized within the system by carbon capturing unit. The ammonia is synthesized on board which is further mixed with water and aqueous ammonia is utilized as an absorbent in the carbon capturing unit. The proposed system has the capability to capture 97131 tonnes/year of carbon emission. The Canadian government has implemented a tax of \$20/tonne of carbon emissions (“CBC News |What is a carbon tax, and will it make a difference?,” n.d.).

$$\dot{C}_{total} = \dot{m}_{CO_2} \times \dot{C}_{CO_2, tax} \quad (12)$$

here,  $\dot{C}_{total}$  represents the total cost which is reduced by capturing carbon dioxide in terms of saving carbon emissions taxes,  $\dot{m}_{CO_2}$  denotes the total flow rate of carbon dioxide which is captured by the employed carbon capturing unit and  $\dot{C}_{CO_2, tax}$  symbolizes the amount of tax implemented by the Canadian government on carbon emissions.

##### 4.2. CO<sub>2</sub> emissions analysis

Due to the implementation of the carbon emissions taxes, every single industry is looking to eradicate the greenhouse gas emissions because these emissions carry several drawbacks such as polluting environment, limiting the production capacities and carbon taxes

as well. The flow rates of the major stream within the system with CO<sub>2</sub> emissions are arranged in Table 2. The left side of the table presents the feed streams data in terms of flow rates and CO<sub>2</sub> emissions while right side of the table exhibits the stream names, flow rates and CO<sub>2</sub> emissions included in the product streams data.

##### 4.3. Data for cost analysis and optimized energy saving

The data for energy saving in terms of flow and cost is arranged in Table 3. It represents the actual and targeted values of flow rates and cost in the table. Thus, as the targeted values are achieved, the available saving is calculated which provides with the percentage of actual data after the energy saving analysis. This energy saving is conducted on the carbon capturing unit using the Aspen Plus software. The table demonstrates that it can offer 54.09–69.89% of saving in terms of flow data while from 54.11 to 69.89% saving in terms of cost in million dollars per year.

The equipment and installation costs of the system's major types of equipment are exhibited in Fig. 3. The equipment costs and installation costs can be depicted from the significant components of the system. Aspen Plus version 9.0 is utilized for the cost and sizing analyses. Different color schemes are used in the figure to represent equipment and installation costs separately.

## 5. Results and discussion

This section presents the key findings of the thermodynamic analysis of the proposed system. Aspen Plus software tool is used to simulate the designed system. Numerous parametric studies are conducted for each major subsystem such as steam methane reforming, autothermal reforming, ammonia synthesis, conversions rates, power production and carbon capturing. This novel integration revealed some enormous results such as high efficiencies for the overall system with the idea of multigeneration

**Table 2**  
CO<sub>2</sub> emission flow rate in the respective streams.

	Feed stream name	Flow rate (kg/s)	CO <sub>2</sub> emissions (kg/s)		Product stream name	Flow rate (kg/s)	CO <sub>2</sub> emissions (kg/s)
Feed streams data	S0	11.87	0.00	Product streams data	S2	11.87	0.00
	S3	1.80	0.00		S3	7.09	0.00
	S5	2.43	0.00		S6	2.43	0.00
	S10	0.16	4.01		S12	0.06	0.00
	S18	2.78	0.00		S15	0.02	0.00
	S33	0.32	8.02		S38	0.07	0.00
	S39	0.64	16.04		S49	0.53	0.00
	S44	3.31	3.08		S52	0.59	0.00
	S54	0.68	0.00		S53	0.68	0.00
	S66	6.41	0.00		S54	0.68	0.00
	S67	7.17	0.00		S70	0.77	0.69
					S71	8.13	0.00

**Table 3**  
The data for the energy saving in terms of flow and cost.

Flow data				
	Actual	Targeted	Available Savings	% of Actual
Total Utilities (W)	5412000	2111000	3301000	60.99
Heating Utilities (W)	2361000	710900	1650000	69.89
Cooling Utilities (W)	3051000	1400000	1651000	54.09
Cost data				
	Actual	Targeted	Available Savings	% of Actual
Total Utilities (\$ Millions/Yr)	0.41	0.16	0.24	59.61
Heating Utilities (\$ Millions/Yr)	0.14	0.04	0.10	69.89
Cooling Utilities (\$ Millions/Yr)	0.26	0.12	0.14	54.11

which reveals a better energy solution. This idea also carries an advantage of onboard ammonia production to capture the CO<sub>2</sub> emissions emitted by the steam reforming section. The state point properties comprising of temperatures, pressures, flow rates, enthalpies, entropies and exergies are tabulated in Table 4.

### 5.1. Effect of different parameters on hydrogen production

The effect of methane flow rate investigated against the heat absorbed by steam methane reforming reactor and hydrogen flow rate and shown in Fig. 4. The significance of this study is to examine

**Table 4**  
State point table including temperatures, pressures, flow rates, enthalpies, entropies and exergies.

State point	From	To	Temperature (°C)	Pressure (kPa)	Molar Enthalpy (kJ/mol)	Molar Entropy (kJ/kmol.K)	Molar Flow Rate (mol/s)	Volumetric Flow Rate (m <sup>3</sup> /s)	Exergy flow rate (kW)
S0		B1A	750	100	-346.4	6.1	280	0.16	9147.6
S1	B1A	B1B	750.1	150	-346.4	6.1	280	0.16	9157.2
S2	B1B		100	150	-406.4	-88.5	280	0.14	248.4
S3		B1B	25	500	-289	-171.3	100	0.00	0.9
S4	B1B	B1C	700	500	-217	-15	100	1.62	2545.6
S5		B1B	25	100	-289	-171.3	135	0.00	0
S6	B1B		675.1	100	-217.9	-2.6	135	10.64	2808.7
S7	B1C	B2A	700	500	-217	-15	10	0.16	254.6
S8	B1C	B2C	700	500	-217	-15	10	0.16	254.6
S9	B1C	B4D	700	500	-217	-15	80	1.29	2036.5
S10		B2A	15	100	-74.9	-81.7	10	0.24	-0.3
S11	B2A	B2B	700	500	-7.5	48.8	40	0.65	544.8
S12	B2B		700	500	19.9	21.4	30	0.49	404.3
S13	B2B	B2C	700	500	-89.7	112	10	0.16	140.4
S14	B2C	B2D	450	1440	-181.1	17.4	20	0.08	253.1
S15	B2D		450	1440	12.5	3.8	10	0.04	113.1
S16	B2D	B4A	450	1440	-374.7	19.4	10	0.04	139.6
S18		B3A	41.9	101.3	0.5	5.9	96.4	2.49	1.3
S19	B3A	B3B	386.1	810.6	10.8	10.6	96.4	0.65	859.5
S20	B3B	B3C	-145.6	810.6	-5.2	-39.2	96.4	0.12	743.5
S21	B3C	B3D	-149	506.6	-5.2	-35.5	96.4	0.19	639.2
S22	B3D	B3B	-178.8	506.6	-11.2	-101.3	75.6	0.00	1442
S23	B3D	B3B	-165.2	506.6	-12	-100.2	20.8	0.00	380.4
S26	B3B	B3F	229.5	506.6	6	2	75.6	0.63	410.2
S27	B3B	B3E	25	506.6	0	-12.2	20.8	0.10	82.9
S28	B3E	B3H	532.2	10000	16.1	-6.1	20.8	0.01	380.3
S29	B3H	B4A	532.2	10000	16.1	-6.1	10.4	0.01	190.1
S30	B3H	B4E	532.2	10000	16.1	-6.1	10.4	0.01	190.1
S31	B3F	B3G	103.3	111.5	2.3	6.1	75.6	2.12	37.2
S33		B4A	15	10000	-76.7	-124.7	20	0.00	220.3
S34	B4A	B4B	950	10000	-51.8	46.3	70.4	0.07	1987.5
S35	B4B	B4E	950	10000	-207	-30.7	10	0.01	401.5
S36	B4B	B4C	950	10000	-26.3	55	60.4	0.06	1646.7
S37	B4C	B4F	950	10000	-81	94.8	30	0.03	836.8
S38	B4C		950	10000	27.7	4.2	30.4	0.03	809.7
S39		B4E	15	100	-74.9	-81.7	40	0.96	-1.1
S40	B4D	B4E	700	500	-217	-15	10	0.16	254.6
S41	B4D	B4F	700	500	-217	-15	70	1.13	1781.9
S42	B4E	B4F	950	10000	-3.3	34.7	140.4	0.15	3789.2
S43	B4F	B4G	450	1440	-100.2	13.5	240.4	1.01	2909.1
S44	B4G		450	1440	-374.7	19.4	70	0.29	976.9
S45	B4G	B5B	450	1440	12.5	4	170.4	0.71	1928.1
S47	B3G	B5A	30	111.5	0.1	-0.2	75.6	1.71	18
S48	B5A	B5B	30	111.5	0.1	-0.2	56.7	1.28	13.5
S49	B5A		30	111.5	0.1	-0.2	18.9	0.43	4.5
S50	B5B	B5C	350	5000	-13.4	-52.3	147.4	0.15	1978.7
S51	B5C	B5D	350	5000	-33.4	-102.7	79.7	0.08	1088.9
S52	B5C		350	5000	9.6	-6	67.8	0.07	870.4
S53	B5D		350	5000	-33.4	-102.7	39.8	0.04	544.4
S54	B5D		350	5000	-33.4	-102.7	39.8	0.04	544.4
S55	B6A		25	100	-289	-171.3	135	0.00	0
S56	B6B	B6A	32.6	8000	-288.2	-169.2	122.1	0.00	23.9
S57	B6A	B6C	645.2	8000	-220.3	-41.4	122.1	0.11	3662.6
S58	B6C	B6A	371	800	-229.9	-35.1	122.1	0.81	2258.3
S60	B6A	B6D	645.2	800	-219.3	-21.3	122.1	1.16	3060.2
S61	B6D	B6E	197.4	5	-235.9	-3.8	122.1	95.54	390.2
S63	B6E	B6B	30	5	-288.6	-169.8	122.1	0.00	0.2
S64		B6E	25	100	-289	-171.3	2497.9	0.05	-0.1
S65	B6E		54.6	100	-286.5	-163	2497.9	0.05	299.6
S66		B2	25	100	-285.8	-163.2	356	0.01	0
S67	B7A	B7B	26.7	101.3	-265.4	-166	400	0.01	0.1
S68	B7B		15.6	101.3	-19.6	0.4	37.1	0.88	0.2
S69	B7B	B7C	15.6	101.3	-322.6	-201	379	0.01	91.1
S70	B7C		60	101.3	-352.1	-0.1	12.1	0.33	9.7
S71	B7C		60	101.3	-291.4	-173.8	396.8	0.01	-180.6

the steam methane reforming system under different conditions. This study can also help to scale up the designed system. It can be depicted from the figure that methane flow rate shows a positive effect on the heat absorbed by steam methane reforming reactor

and hydrogen flow rate. The rise in the methane flow rate supports the hydrogen production rate and higher production rate gives rise to the heat absorbed by the endothermic reaction. The amount of carbon monoxide produced in the steam methane reforming is

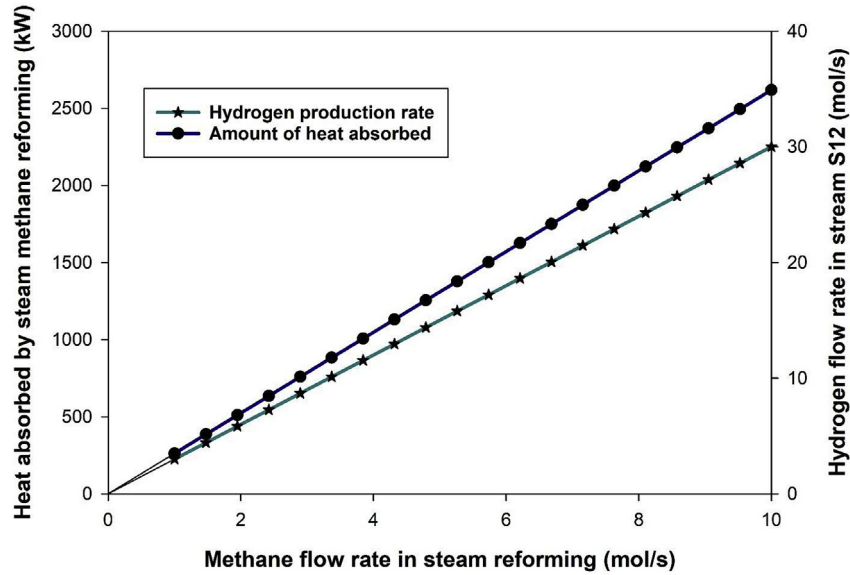


Fig. 4. Investigation of methane flow rate effect on the heat absorbed by steam methane reforming reactor and hydrogen flow rate.

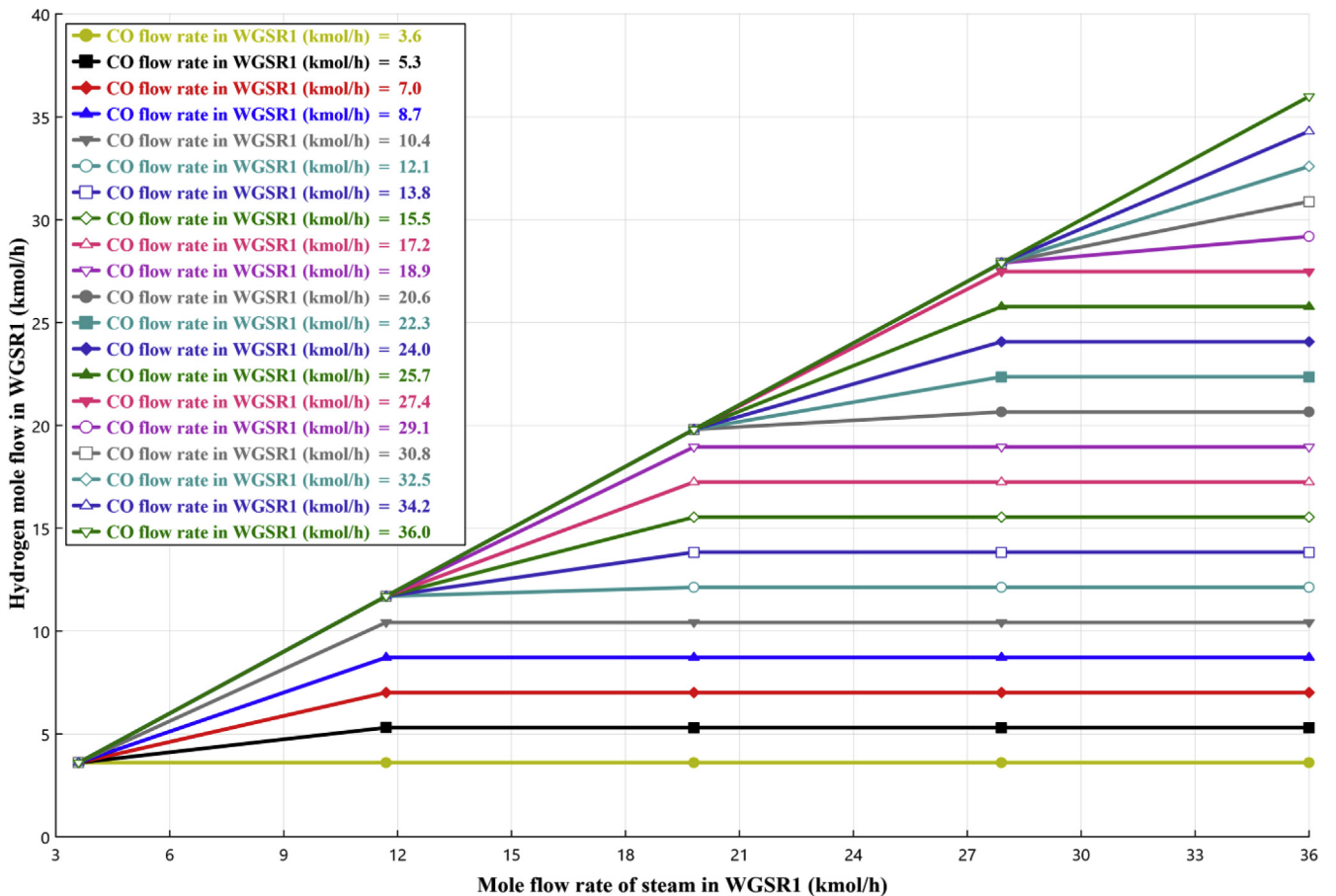


Fig. 5. Effect of steam and carbon monoxide flow rate on hydrogen production.

further converted to the carbon dioxide by reacting it with steam in water gas shift reactor. Fig. 5 exhibits the effect of the carbon monoxide and steam flow rate on hydrogen production. The flow rate of steam is drawn on x-axis while the change in carbon monoxide flow rate is shown in the legends with different colored line and results of hydrogen production are plotted on y-axis. Figure depicts that the flow rate of carbon monoxide and steam supports the hydrogen production and gradual increase in the hydrogen production rate is shown in figure.

Fig. 6 displays the methane flow rate effect on the hydrogen flow rate and heat absorbed by autothermal methane reforming reactor. The range of the natural gas flow rate is taken in the range of 0–20 mol/s which results in the hydrogen production rate from 22 to 32 mol/s and endothermic reaction absorbs the heat in the range of 400–1400 kW. Figure displays that methane flow rate gives rise to the hydrogen production rate and in order to deal with a higher flow rate, the reactor absorbs more amount of heat. To investigate the autothermal methane reforming reactor under different flow rates is the objective and significance of this study. The flow rate of

steam and carbon monoxide in the water gas shift reactor 2 is plotted again the carbon dioxide and hydrogen flow rate in Fig. 7. The flow rate of the input stream including steam and carbon monoxide is considered in the range of 0–140 mol/s. Water gas shift reactor 2 is a novel integration with autothermal reforming thus, this study has the significance to investigate its performance. It can be depicted from the figure that the flow rate of the steam and carbon dioxide has positive effect on the hydrogen production. The carbon dioxide produced in this reactor is captured in the carbon capturing unit.

## 5.2. Investigation on ammonia synthesis and conversion rates

Both hydrogen and nitrogen are supplied to the ammonia synthesis reactor. The ammonia synthesis reaction takes place at the temperature of 350 °C and pressure of 50 bar. The conversion rate of the ammonia synthesis reactor is taken as 70%. The effect of hydrogen flow rate is investigated on the heat released by ammonia reactor and ammonia production rate in Fig. 8. Ammonia synthesis

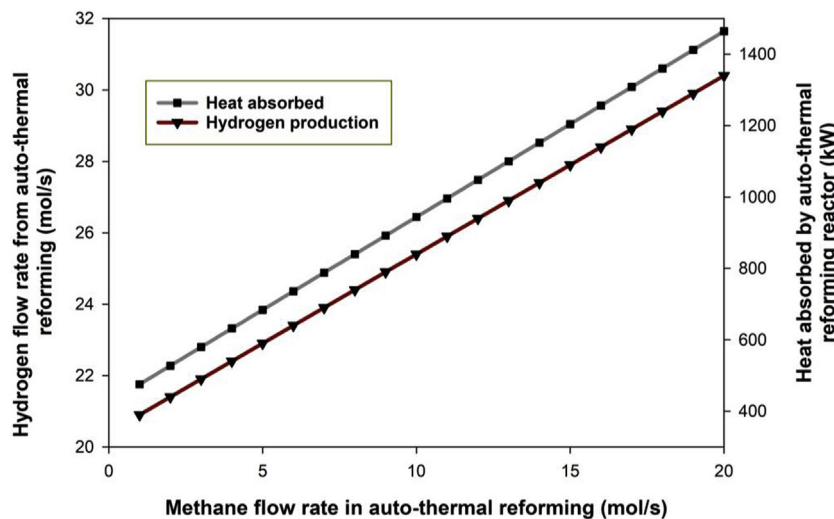


Fig. 6. Methane flow rate effect on the heat duty and hydrogen flow rate.

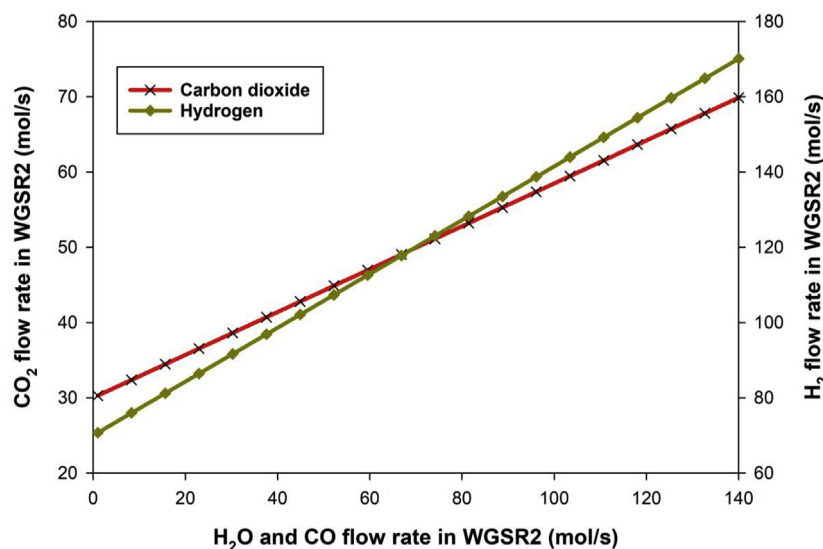


Fig. 7. Effect of steam and carbon monoxide flow rate on hydrogen production in WGSR2.

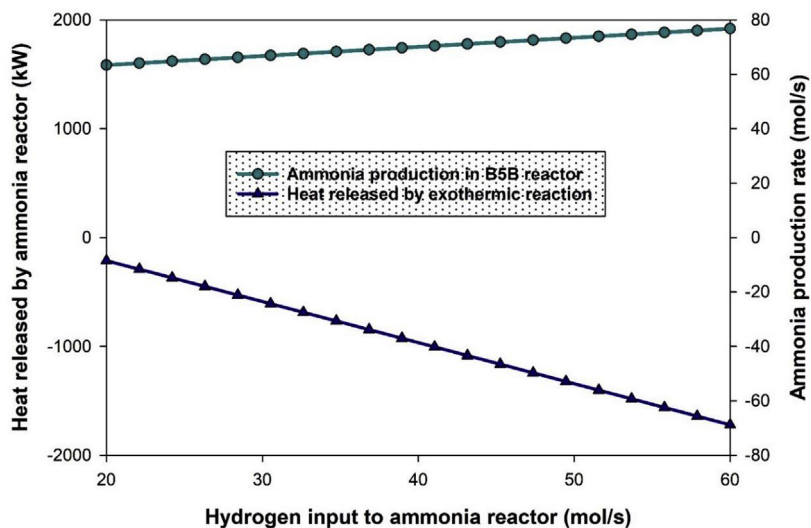


Fig. 8. Hydrogen flow rate effect on heat duty and ammonia synthesis.

is an exothermic reaction which releases heat. The endothermic reaction is shown with positive while exothermic reaction is given as negative heat in the Aspen plus. Thus, with the increase in the hydrogen flow rate, the heat absorbed by the reaction rises and an increase in the input supports the ammonia production rate.

Fig. 9 displays the effect of conversion rate on the ammonia production rate and heat released by ammonia synthesis. The conversion rate is considered in the range of 0.5–1. The flow rate of ammonia and unreacted gases are taken on one side of y-axis while the heat released by the reaction is taken on the other side of y-axis. It can be depicted that with the rise in conversion rate, the heat absorbed by the reaction increases, the ammonia production rate rises and unreacted gases decreases. Fig. 10 exhibits the effect of nitrogen and hydrogen flow rates on the ammonia production flow rate. A 3D representation is shown to display this effect of flow rates on ammonia synthesis. The nitrogen flow rate is taken on x-axis while hydrogen flow rate is considered on y-axis and the effect of these two parameters is investigated on the ammonia production capacity. The nitrogen flow rate is taken in the range of 20–100 mol/s and hydrogen flow rate is considered in the range of 50–250 mol/s. The significance of this figure is to investigate the ammonia

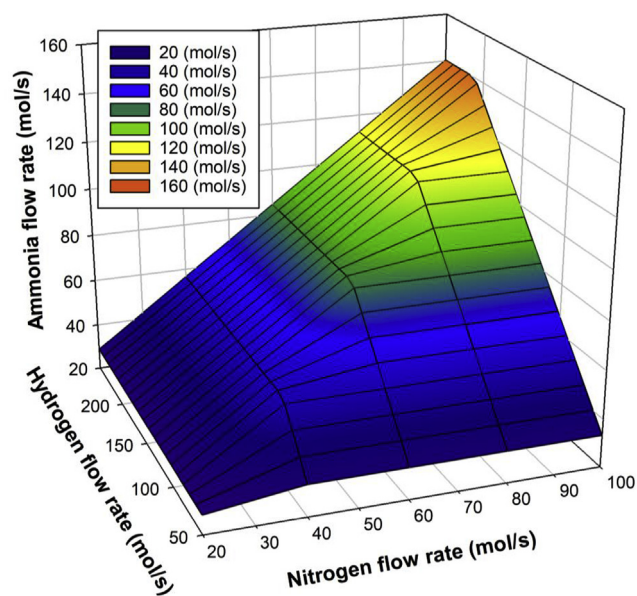


Fig. 10. Nitrogen and hydrogen flow rate effect on ammonia synthesis.

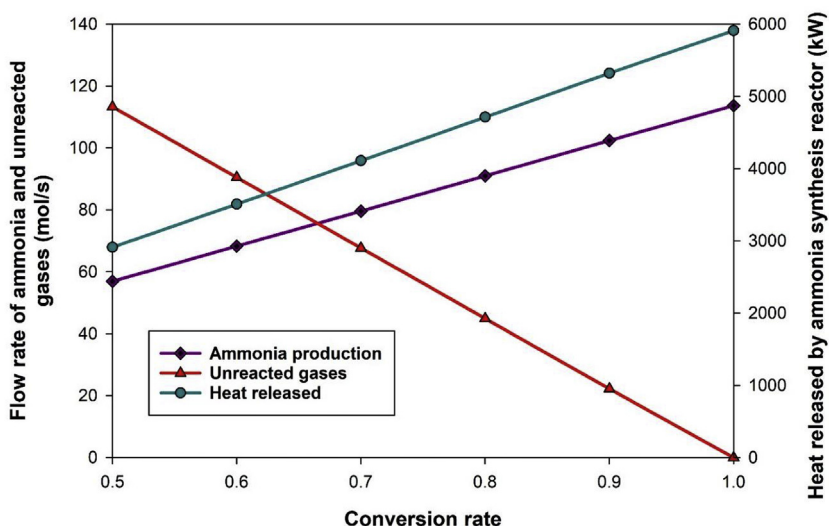


Fig. 9. Conversion rate effect on the heat duty and flow rate of ammonia and unreacted gases.

production capacity at the operating conversion rate of 70%, respectively.

### 5.3. Parametric studies for the power production

Similar to the other subsystems, some parametric studies are conducted on the reheat Rankine cycle as well. The significance of these studies is to investigate the effect of system operating parameters on the input temperature of the reheat Rankine cycle and power produced by high and low-pressure turbines. The effect of mole flow rate of the molten salt is investigated against the enthalpy flow rate of steam S6 and the steam input temperature to the reheat Rankine cycle in Fig. 11. The molten salt is considered in the range of 230–300 mol/s. It can be depicted from the figure that increases in the molten salt flow rate results in the decreased molar enthalpy and an increase in the input temperature to the reheat Rankine cycle (RRC).

The effect of the flow rate of steam to the reheat Rankine cycle against the power production by the high and low pressure turbines is displayed in Fig. 12. The flow rate of water is considered in the range of 100–150 mol/s. This study also helps to achieve the

optimum condition of working flow rate for the reheat Rankine cycle. The power produced by the high-pressure turbine increases from 300 to 1400 kW with a rise in water flow rate while the power produced by the low-pressure turbine increases from 1300 to 2450 kW with rise in water flow rate.

### 5.4. Carbon capturing and heat duty studies

The ammonia is synthesized on board for carbon capturing unit. A part of ammonia produced is mixed with water and aqueous ammonia is used as absorbent to the carbon capturing unit. The flow rate of aqueous ammonia is taken in the range of 20–40 mol/s. The aqueous ammonia absorbs carbon dioxide in the absorption step B7B and the unreacted carbon dioxide and ammonia are separated in the stripper section. Aspen flow shows the absorbed heat and positive while the amount of heat released is shown with a negative sign. It can be depicted from Fig. 13 that amount of heat absorbed and released increased with the increase in ammonia flow rate.

Fig. 14 displays the amount of heat absorbed or released by the major reaction steps of the designed system. The major

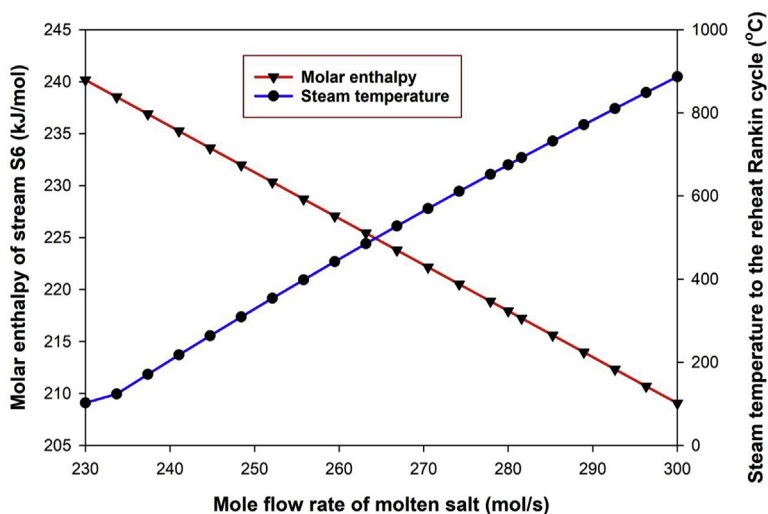


Fig. 11. Molten salt flow rate effect on molar enthalpy and input temperature of RRC.

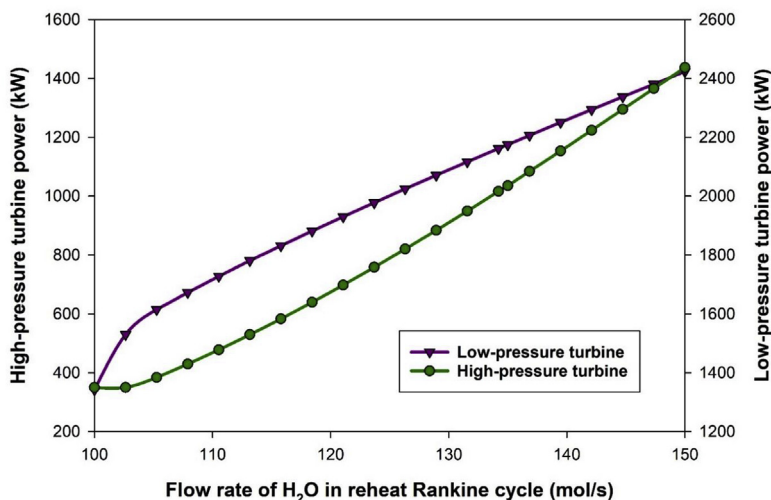


Fig. 12. Water flow rate effect on the power produced by high and low-pressure turbine.

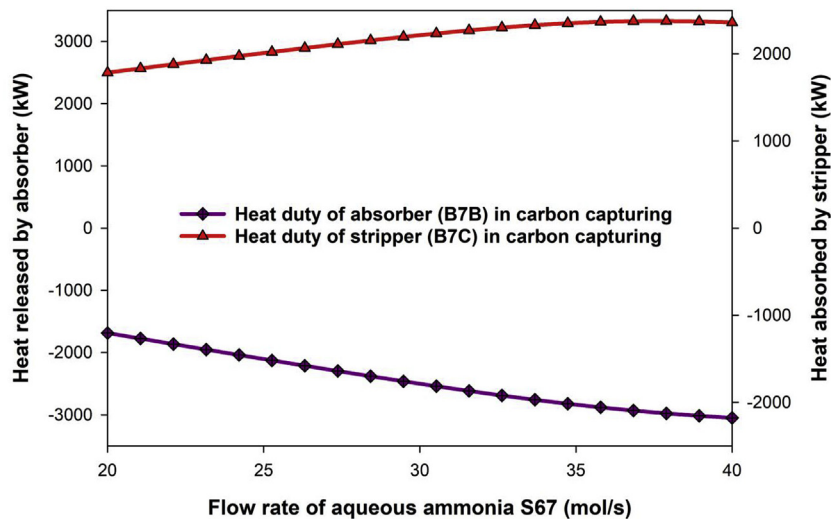


Fig. 13. Heat released and absorbed by the carbon capturing system.

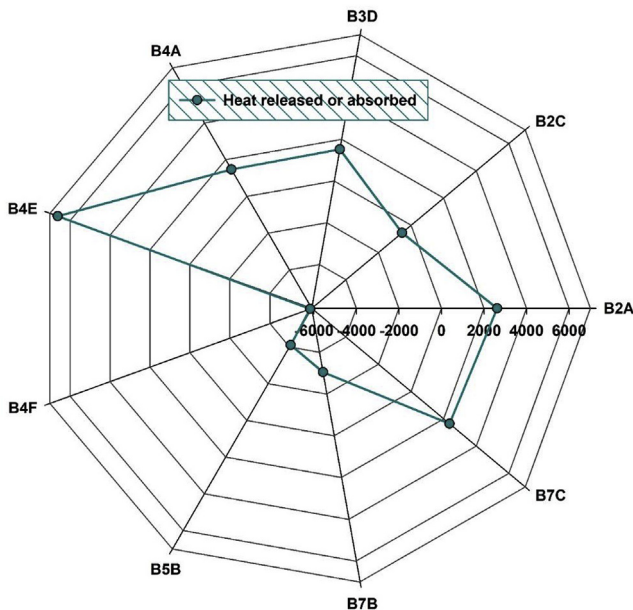


Fig. 14. The amount of heat released and absorbed by the major system components.

components considered in this study are steam-autothermal reforming reactors, water gas shift reactors, ammonia synthesis reactor, distillation column, absorber and stripper. The endothermic reaction is shown as positive while the exothermic reaction shown as negative heat in the Aspen plus. Figure represents all the major endothermic and exothermic reactions occurring in the designed system.

### 5.5. Overall results and efficiencies investigation

The significant results of the overall system and the efficiencies investigations are presented in this section. The major outcomes of the designed system are arranged in Table 5. The key results such as hydrogen production, hot water flow rate, power production and ammonia synthesis are tabulated in the table. Fig. 15 exhibits the effect of the ambient temperature on the energy and exergy efficiencies of the overall system. The overall energy and exergy

Table 5

Major outcomes of the proposed system.

Parameter	Value	Unit
Hydrogen production rate	70	mol/s
Ammonia production rate	39.8	mol/s
Power production	515	kW
Hot water flow rate	45	kg/s
Overall energy efficiency	53.4	%
Overall exergy efficiency	45.0	%

efficiencies are found to be 53.4% and 45.0%. The temperature range considered for this parametric study is taken from 0 to 40 °C. It can be depicted from figure that ambient temperature does not effect the energy efficiency of the overall system as 53.4% while exergy efficiency increases from 38% to 48%. The significance of this study is to investigate the system efficiencies under the different reference temperatures.

### 5.6. Validation

This study presents a new approach for the energetically enhanced integrated system including steam-autothermal hybrid reforming system including onboard carbon capturing. Siddiqui and Dincer (2017) conducted a study based on the solar heliostat for multigeneration and found the energetic and exergetic efficiencies 39.1% and 38.7%, another study conducted by Ishaq et al. (2018) developed a solar energy based multigeneration system and found the overall efficiencies of 49% and 48.2% while the study proposed in current study achieved the energetic and exergetic efficiencies of 53.4% and 45.0% respectively.

## 6. Conclusions

A novel integration of solar based steam-autothermal hybrid reforming system is proposed in this study. The amount of carbon dioxide released in the steam methane reforming is employed to the autothermal reforming system. Both, steam and carbon dioxide based autothermal reforming are integrated with the designed system. An innovative idea of the autothermal reforming integration with water gas shift reactor is proposed in this study and produced carbon dioxide is captured through carbon capturing

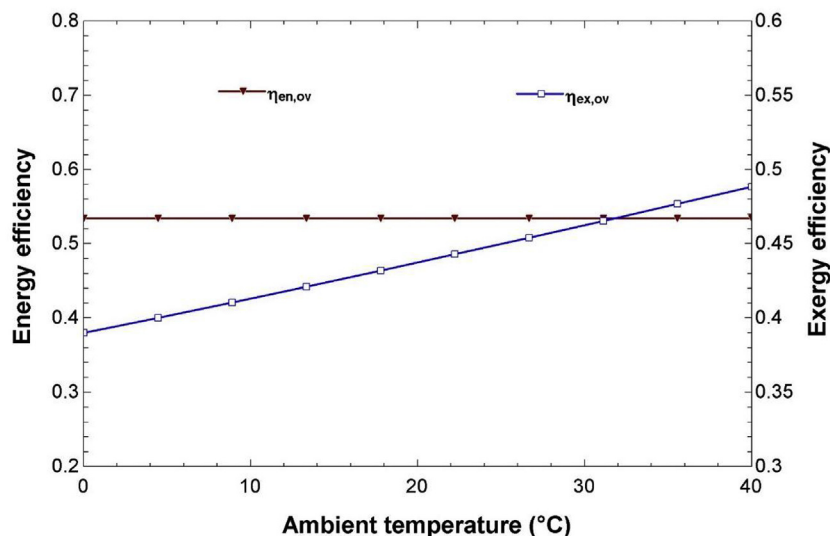


Fig. 15. Ambient temperature effect on energy and exergy efficiencies of the overall system.

unit. The major subsystems of the designed system are solar heliostat field, steam methane reforming, autothermal reforming, cryogenic air separation unit, ammonia synthesis, reheat Rankine cycle and carbon capturing system. For future studies, some other systems which are able to replace the reheat Rankine cycle and aqueous ammonia based carbon capturing must be investigated to overcome the high exergy destruction rates. Furthermore, investigating the sizes and dimensions for each component such as reactors, pumps, separators and heat exchangers is also recommended for future studies. The key findings of the proposed system are as follows:

- The proposed system has the capability to produce 70 mol/s of hydrogen from steam and autothermal reforming system.
- Power produced by the reheat Rankine cycle covers the electrical input requirements and generates a final output power of 515 kW.
- The additional heat available in the condenser of the reheat Rankine cycle is utilized to produce 45 kg/s of hot water.
- To capture the carbon dioxide produced by the natural gas reforming, ammonia is synthesized on board with a flow rate of 39.8 mol/s.
- The proposed system captures 97131 tonnes/year of carbon emissions and saves \$1.9 million per year of carbon emissions taxes.

## Nomenclature

$\dot{C}$	cost coefficient (\$/year)
ex	specific exergy (kJ/kg)
en	specific energy (kW)
$\dot{E}x_{dest}$	exergy destruction rate (kW)
h	specific enthalpy (kJ/kg)
LHV	lower heating value (kJ/kg)
$\dot{m}$	mass flow rate (kg/s)
$\dot{m}_{CO_2}$	CO <sub>2</sub> flow rate (tonne/year)
T	temperature (°C)
$\dot{Q}$	heat rate (kW)
$\dot{W}$	work rate (kW)

## Greek letters

$\eta_{en}$	energy efficiency
-------------	-------------------

$\eta_{ex}$  exergy efficiency

## Subscripts

1, 2, ... 71	state points
B#	block name
S	Stream name
e	exit
i	input
dest	destroyed
ov	overall

## Acronyms

ATR	Autothermal reforming
CASU	Cryogenic air separation unit
EIA	Energy Information Administration
ORC	Organic Rankine cycle
RRC	Reheat Rankine cycle
SAHRS	Steam-autothermal hybrid reforming system
SMR	Steam methane reforming
SHF	Solar heliostat field
WGSR	Water gas shift reactor

## References

- Al-Bassam, A.M., Conner, J.A., Manousiouthakis, V.I., 2018. Natural-gas-derived hydrogen in the presence of carbon fuel taxes and concentrated solar power. *ACS Sustain. Chem. Eng.* 6 (3), 3029–3038. <https://doi.org/10.1021/acssuschemeng.7b02745>.
- Atif, M., Al-Sulaiman, F.A., 2018. Energy and exergy analyses of recompression Brayton cycles integrated with a solar power tower through a two-tank thermal storage system. *J. Energy Eng.* 144 (4). [https://doi.org/10.1061/\(ASCE\)EY.1943-7897.0000545](https://doi.org/10.1061/(ASCE)EY.1943-7897.0000545).
- CBC News. What is a carbon tax, and will it make a difference? (n.d.). <https://www.cbc.ca/news/technology/federal-carbon-tax-1.4874706>.
- Colucci, J.A., 2006. Hydrogen production using autothermal reforming of biodiesel and other hydrocarbons for fuel cell applications. *Sol. Energy* 2006, 483–484. <https://doi.org/10.1115/ISEC2006-99018>.
- Ding, Y., Alpay, E., 2000. Adsorption-enhanced steam methane reforming. *Chem. Eng. Sci.* 55. <https://pdf.sciencedirectassets.com/271348/1-s2.0-S0009250900X01339>.
- EIA, 2019. U.S. Energy Information Administration (EIA) - Total Energy Monthly Data [https://doi.org/DOE/EIA-0035\(2019/1\)](https://doi.org/DOE/EIA-0035(2019/1)).
- Hagh, B.F., 2004a. Comparison of autothermal reforming for hydrocarbon fuels. In: *ACS Division of Fuel Chemistry*, vol 49.
- Hagh, B.F., 2004b. Stoichiometric analysis of autothermal fuel processing. *J. Power Sources* 130 (1–2), 85–94. <https://doi.org/10.1016/j.jpowsour.2003.11.041>.
- Ishaq, H., Dincer, I., 2019. Investigation of an integrated system with industrial thermal management options for carbon emission reduction and hydrogen and

- ammonia production. *Int. J. Hydrogen Energy*. <https://doi.org/10.1016/j.ijhydene.2019.03.067>.
- Ishaq, H., Dincer, I., Naterer, G.F., 2018. Development and assessment of a solar, wind and hydrogen hybrid trigeneration system. *Int. J. Hydrogen Energy* 43 (52), 23148–23160. <https://doi.org/10.1016/j.ijhydene.2018.10.172>.
- Islam, S., Dincer, I., 2017. Development, analysis and performance assessment of a combined solar and geothermal energy-based integrated system for multi-generation. *Sol. Energy* 147, 328–343. <https://doi.org/10.1016/j.solener.2017.02.048>.
- Jegadheesan, C., Somasundaram, P., Meenakshipriya, B., Vignesh, U.P., 2013. Investigation on the effects of conventional fossil fuel to the environment and research on renewable fuels with reduced emission using biodiesel, diethyl ether and hydrogen. *Nat. Environ. Pollut. Technol.* 12 (4), 661–666.
- Kim, D.Y., Lee, H.M., Min, S.K., Cho, Y., Hwang, I.C., Han, K., Kim, K.S., 2011. CO<sub>2</sub> capturing mechanism in aqueous ammonia: NH<sub>3</sub>-driven decomposition-recombination pathway. *J. Phys. Chem. Lett.* 2 (7), 689–694. <https://doi.org/10.1021/jz200095j>.
- Muradov, N.Z., Veziroğlu, T.N., 2008. “Green” path from fossil-based to hydrogen economy: an overview of carbon-neutral technologies. *Int. J. Hydrogen Energy* 33 (23), 6804–6839. <https://doi.org/10.1016/j.ijhydene.2008.08.054>.
- Raibhole, V.N., Sapali, S.N., 2012. Simulation and parametric analysis of cryogenic oxygen plant for biomass gasification. *Mech. Eng. Res.* 2 (2). <https://doi.org/10.5539/mer.v2n2p97>.
- Ray, A., 2015. Cryogenic separation of atmospheric air in a typical Air Separation Unit (ASU) using Hampson-Linde cycle. *Int. J. Eng. Tech. Res. (IJETR)* 3 (12), 81–85.
- Sheu, E.J., Mitsos, A., 2013. Optimization of a hybrid solar-fossil fuel plant: solar steam reforming of methane in a combined cycle. *Energy* 51, 193–202. <https://doi.org/10.1016/j.energy.2013.01.027>.
- Siddiqui, O., Dincer, I., 2017. Analysis and performance assessment of a new solar-based multigeneration system integrated with ammonia fuel cell and solid oxide fuel cell-gas turbine combined cycle. *J. Power Sources* 370, 138–154. <https://doi.org/10.1016/j.jpowsour.2017.10.008>.
- Wang, Z., Naterer, G.F., 2014. Integrated fossil fuel and solar thermal systems for hydrogen production and CO<sub>2</sub> mitigation. *Int. J. Hydrogen Energy* 39, 14227–14233. <https://doi.org/10.1016/j.ijhydene.2014.01.095>.
- Wu, Y., Wang, Y., Zeng, Q., Gong, X., Yu, Z., 2009. Experimental study on capturing CO<sub>2</sub> greenhouse gas by mixture of ammonia and soil. *Front. Chem. Eng. China* 3 (4), 468–473. <https://doi.org/10.1007/s11705-009-0257-7>.
- Xu, Y., Zhao, M., Qiu, Y., Zhou, C., Gu, P., Xiang, W., 2017. Performance of coal power generation integrating coal based solar energy storage with CO<sub>2</sub> capture. *Taiyangneng Xuebao/Acta Energetica Solaris Sinica* 38 (1).
- Yan, Y., Li, H., Li, L., Zhang, L., Zhang, J., 2018. Properties of methane autothermal reforming to generate hydrogen in membrane reactor based on thermodynamic equilibrium model. *Chem. Eng. Process. Process Intensification* 125, 311–317. <https://doi.org/10.1016/j.cep.2018.01.010>.
- Zheng, R., Diver, R., Caldwell, D., Fritz, B., Cameron, R., Humble, P., et al., 2015. Integrated solar thermochemical reaction system for steam methane reforming. In: *Energy Procedia*, vol 69, pp. 1192–1200. <https://doi.org/10.1016/j.egypro.2015.03.204>.